

Marginal rays in tapered gradient-index lenses

José Manuel Rivas-Moscato

Carlos Gómez-Reino, MEMBER SPIE

María Victoria Pérez Martín

Carmen Bao Varela

Universidade de Santiago de Compostela

Escola de Optica e Optometría and

Facultade de Física

Laboratorio de Optica, Departamento de

Física Aplicada

E-15782 Santiago de Compostela, Spain

E-mail: facgrc@usc.es

Abstract. Marginal rays are used to study the limitations of the spatial and angular extents of light beams by stops and apertures in tapered gradient-index lenses. The results are applied to two kinds of taper functions and compared to selfoc lenses. © 2002 Society of Photo-Optical Instrumentation Engineers. [DOI: 10.1117/1.1430418]

Subject terms: gradient-index; lenses; geometric optics; apertures; ray propagation; vignetting.

Paper 010042 received Feb. 20, 2001; revised manuscript received Aug. 13, 2001; accepted for publication Aug. 16, 2001.

1 Introduction

It is well known that for any optical system, including gradient-index (GRIN) systems, it is not enough to be able to predict the image position and its size. Other important properties of an image include, for instance, the brightness and size of the field of view. These topics require a study of the limitations of the spatial and angular extents of light beams by stops and apertures. Even if the optical system under consideration accepts light rays that are not paraxial, it is usually sufficient to treat stops and apertures and related effects by using methods of paraxial optics.¹⁻⁵ Marginal rays are of particular importance for studying basic magnitudes and topics related to the limitations of the spatial and angular extents of light beams propagating in optical systems.⁶⁻⁹ Thus, the main task of this paper is to evaluate the effective radius and the numerical aperture as well as the aperture stop and the pupils of a tapered GRIN lens by marginal rays. The knowledge of these parameters should be useful when designing GRIN lens systems.

2 Statement of the Problem

We consider a tapered GRIN lens with rotational symmetry of radius a and length d limited by plane parallel faces perpendicular to the z axis whose refractive index profile is given by

$$n^2(r, z) = \begin{cases} n_0^2[1 - g^2(z)r^2] & \text{for } r \leq a \text{ and } 0 \leq z \leq d \\ 1 & \text{otherwise,} \end{cases} \quad (1)$$

provided that the GRIN lens is surrounded by a vacuum or free space, where n_0 is the index at the lens axis, $g(z)$ is the gradient parameter, and $r = (x^2 + y^2)^{1/2}$.

The paraxial ray equations at any transverse plane inside the tapered GRIN lens can be expressed as⁵

$$r(z) = r_0 H_f(z) + \dot{r}_0 H_a(z), \quad (2a)$$

$$\dot{r}(z) = r_0 \dot{H}_f(z) + \dot{r}_0 \dot{H}_a(z), \quad (2b)$$

where r_0 and r and \dot{r}_0 and \dot{r} are the position and slope of the ray at the input and z planes, respectively, and the dot represents the derivative with respect to z .

Likewise, H_f and \dot{H}_f and H_a and \dot{H}_a are the position and slope at z of the field and axial rays, respectively. They can be written as

$$\begin{aligned} H_a(z) &= [g_0 g(z)]^{-1/2} \sin \left[\int_0^z g(z') dz' \right] \\ &= -[g_0 g(z)]^{-1} \dot{H}_f(z), \end{aligned} \quad (3a)$$

$$\begin{aligned} H_f(z) &= [g_0 / g(z)]^{1/2} \cos \left[\int_0^z g(z') dz' \right] \\ &= \frac{g_0}{g(z)} \dot{H}_a(z), \end{aligned} \quad (3b)$$

where g_0 is the value of $g(z)$ at $z=0$. Both rays are related to each other by the Lagrange invariant

$$\dot{H}_a(z) H_f(z) - H_a(z) \dot{H}_f(z) = 1. \quad (4)$$

For a GRIN lens illuminated by an on-axis point source at a distance d_1 from the input face (Fig. 1), the ray slope at this face is given by

$$\dot{r}_0 = \frac{\dot{r}(0)}{n_0} = \frac{r_0}{n_0 d_1}. \quad (5)$$

Substitution of Eq. (5) into Eqs. (2) provides

$$r(z) = r_0 F(z), \quad (6a)$$

$$\dot{r}(z) = r_0 \dot{F}(z), \quad (6b)$$

where

$$F(z) = H_f(z) + \frac{\dot{H}_a(z)}{n_0 d_1}. \quad (7)$$

Equations (6) can also be expressed as

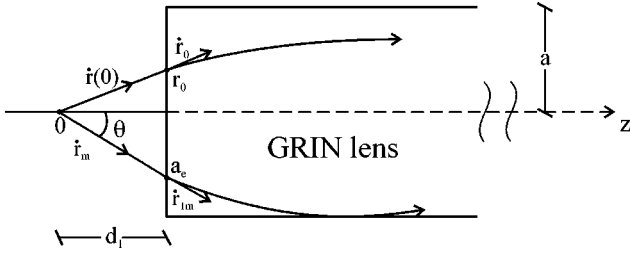


Fig. 1 GRIN lens illuminated by an on-axis point source at a distance d_1 from the input face.

$$r(z) = R(z) \sin \left[\int_0^z g(z') dz' + \delta_0 \right], \quad (8a)$$

$$\dot{r}(z) = g(z) R(z) \cos \left[\int_0^z g(z') dz' + \delta_0 \right], \quad (8b)$$

where

$$R(z) = \left[\frac{\dot{r}_0^2 + g_0^2 r_0^2}{g_0 g(z)} \right]^{1/2}, \quad (9a)$$

$$\delta_0 = \tan^{-1} \left(\frac{g_0 r_0}{\dot{r}_0} \right), \quad (9b)$$

and Eqs. (3), (6), and (7) have been used.

Equations (8) show that the paraxial refracted ray path in the tapered GRIN lens is a sinusoidal path with amplitude $R(z)$ and initial phase δ_0 (Ref. 7).

3 Effective Radius and Numerical Aperture

In a tapered GRIN lens, a ray will be confined if its height satisfies the condition

$$\left[\frac{\dot{r}_0^2 + g_0^2 r_0^2}{g_0 g(z)} \right]^{1/2} \leq a. \quad (10)$$

Equation (10) shows that not all the rays reaching the input face of the lens will be confined through it and then there is an angular limitation in the cone of light entering the lens.

For the paraxial marginal ray Eq. (10) becomes

$$\dot{r}_m^2 + g_0^2 a_e^2 = a^2 g_0 g(z), \quad (11)$$

where a_e and \dot{r}_m are the position and the slope of this ray at the input face.

The marginal ray starting from an off-axis object point at a distance d_1 from the input face (Fig. 2) with position b and slope \dot{r}_{1m} verifies that

$$\left(\frac{\dot{r}_{1m}}{n_0} \right)^2 + g_0^2 a_e^2 = a^2 g_0 g(z), \quad (12)$$

where

$$a_e = b + d_1 \dot{r}_{1m}. \quad (13)$$

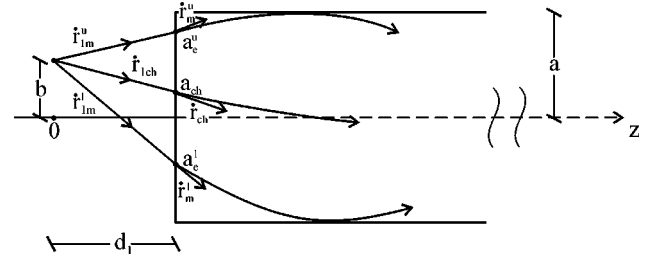


Fig. 2 Limitation of rays in a GRIN lens for an off-axis object point. Subindices m and ch denote marginal and chief rays, and superindices u and l indicate upper and lower marginal rays, respectively.

From Eqs. (12) and (13) it follows that

$$\dot{r}_{1m}^{(u)} = \frac{-n_0^2 g_0^2 b d_1 \pm n_0 [(1 + n_0^2 g_0^2 d_1^2) a^2 g_0 g(z) - g_0^2 b^2]^{1/2}}{1 + n_0^2 g_0^2 d_1^2}, \quad (14)$$

with prescription u is for plus and l is for minus since each object point has upper and lower marginal meridional rays corresponding to the solutions in Eq. (14).

Likewise, the chief ray is the ray in the center of the cone of light from any point of the object (Fig. 2). Equations (12)–(14) show that the slope of the chief ray is

$$\dot{r}_{1ch} = - \frac{n_0^2 g_0^2 d_1 b}{1 + n_0^2 g_0^2 d_1^2}, \quad (15)$$

and its position on the input face of the tapered GRIN lens is

$$a_{ch} = \frac{b}{1 + n_0^2 g_0^2 d_1^2}, \quad (16)$$

the trajectory of the chief ray along the lens can be expressed as

$$\begin{aligned} r_{ch}(z) &= a_{ch}^{(\cdot)} H_f(z) + \dot{r}_{ch}^{(\cdot)} H_a(z) \\ &= \frac{b}{1 + n_0^2 g_0^2 d_1^2} [H_f(z) - n_0 g_0^2 d_1 H_a(z)], \end{aligned} \quad (17)$$

where $\dot{r}_{ch} = \dot{r}_{1ch}/n_0$ and Eqs. (2), (15), and (16) have been used.

Moreover, from Eqs. (13) and (14) we can find the positions of the upper and lower marginal rays on the input face:

$$a_e^{(u)} = \frac{b \pm n_0 d_1 [(1 + n_0^2 g_0^2 d_1^2) a^2 g_0 g(z) - g_0^2 b^2]^{1/2}}{1 + n_0^2 g_0^2 d_1^2}, \quad (18)$$

which determine the effective aperture of the tapered GRIN lens given by

$$EA = \frac{2n_0 d_1 [(1 + n_0^2 g_0^2 d_1^2) a^2 g_0 g(z) - g_0^2 b^2]^{1/2}}{1 + n_0^2 g_0^2 d_1^2}. \quad (19)$$

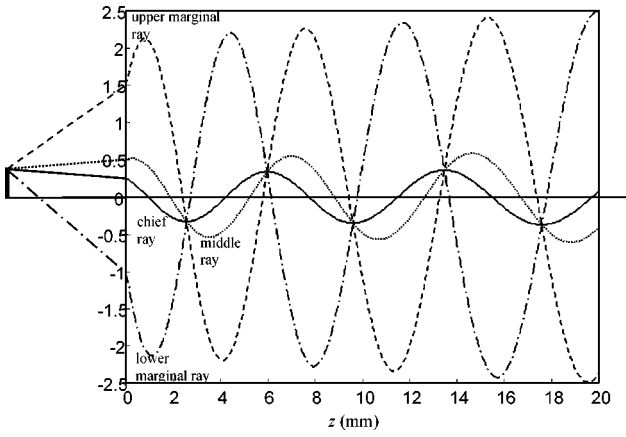


Fig. 3 Representation of meridional ray trace for a linear divergent medium. We show the meridional marginal rays, the chief ray, and a middle ray. Calculations were made for lens radius $a=2.5$ mm, GRIN lens thickness $d=7$ mm, index at the optical axis $n_0=1.5$, $g_0=0.1$ mm⁻¹, $L=100$ mm, object lateral displacement $b=1$ mm, and distance $d_1=5$ mm.

Equation (19) indicates that the effective aperture decreases as b increases. There is a maximum height b_m of the object for which the GRIN lens will not accept any ray. This is so when b is large enough to cancel the effective aperture. From Eq. (19) it follows that

$$b_m = a \left[\frac{g(z)(1 + n_0^2 g_0^2 d_1^2)}{g_0} \right]^{1/2}. \quad (20)$$

Therefore b_m defines the spatial extent of the object, that is, the size of the field of view in the object space.

Equations (14), (16), and (18) for the on-axis point ($b=0$) reduce to

$$\dot{r}_{1m} = \pm n_0 a \left[\frac{g_0 g(z)}{1 + n_0^2 g_0^2 d_1^2} \right]^{1/2}, \quad (21)$$

$$a_{\text{ch}} = 0, \quad (22)$$

$$a_e = d_1 \dot{r}_{1m} = \pm n_0 a d_1 \left[\frac{g_0 g(z)}{1 + n_0^2 g_0^2 d_1^2} \right]^{1/2}. \quad (23)$$

Figure 3 presents an example of ray tracing for a GRIN medium with a linear-divergent profile.

From Eqs. (21) and (22) it follows that the marginal rays generate a revolution light cone around the z axis, subtending at 0 an angle θ (Fig. 1). Then, the input numerical aperture, a quantity specifying the light-gathering power of an optical system, is given by⁸

$$\begin{aligned} \text{NA}_{\text{in}} = \sin \theta &= \left(\frac{a_e^2}{a_e^2 + d_1^2} \right)^{1/2} \\ &= n_0 a \left\{ \frac{g_0 g(z)}{1 + n_0^2 g_0 [a^2 g(z) + d_1^2 g_0]} \right\}^{1/2}. \end{aligned} \quad (24)$$

Likewise, Eq. (23) defines the effective radius of the input face of the GRIN lens for which the rays are confined inside it. Therefore, the evolution of the position and slope of the marginal rays can be written as

$$r_m(z) = a_e F(z), \quad (25)$$

where Eqs. (6) have been used.

In this way, the maximum ray deviation from the central axis corresponds to a height equal to the edge of the GRIN lens in which the slope of the marginal ray is parallel to the z axis. This fact provides the conditions $a_e = a/F(z)$ and $\dot{F}(z) = 0$ for the position and the slope of the marginal rays at the edge of the lens, respectively.

On the other hand, there are conjugate topics related to the image space. They are the output effective radius and the output numerical aperture given by

$$a'_e(d) = \pm n_0 a d_1' \left[\frac{g(d)g(z)}{1 + n_0^2 g^2(d) d_1'^2} \right]^{1/2}, \quad (26)$$

$$\begin{aligned} \text{NA}_{\text{out}}(d) &= \left(\frac{a_e'^2}{a_e'^2 + d_1'^2} \right)^{1/2} \\ &= n_0 a \left\{ \frac{g(d)g(z)}{1 + n_0^2 g(d)[a^2 g(z) + d_1'^2 g(d)]} \right\}^{1/2}, \end{aligned} \quad (27)$$

where d_1' is the image distance measured from the output face of the lens. Note that Eqs. (26) and (27) can be obtained from Eqs. (23) and (24) by replacing g_0 , d_1 , and a_e by $g(d)$, d_1' , and a_e' , respectively.

Input and output numerical apertures are important parameters when we use a GRIN lens as a collimator or focuser in optical connections to evaluate the collimated beam or the point spread function.¹⁰

Finally, another conjugate topic is the size of the field of view for the image space given by

$$b'_m = b_m m_t, \quad (28)$$

where m_t is the transverse magnification of the GRIN lens⁵

$$m_t = H_f(d) + n_0 d_1' \dot{H}_f(d). \quad (29)$$

4 Aperture Stop and Pupils

The aperture stop is the rim of the lens or the stop that physically limits the cone of rays, from the axial point object, passing through an optical system. For the aperture stop in a GRIN lens, the position and the slope of a marginal ray are given by

$$r_m(d_s) = a, \quad (30a)$$

$$\dot{r}_m(d_s) = 0, \quad (30b)$$

where d_s is the position of the aperture stop measured from the input face of the lens (Fig. 4).

From Eq. (25) it follows that Eqs. (30a) and (30b) can be written as

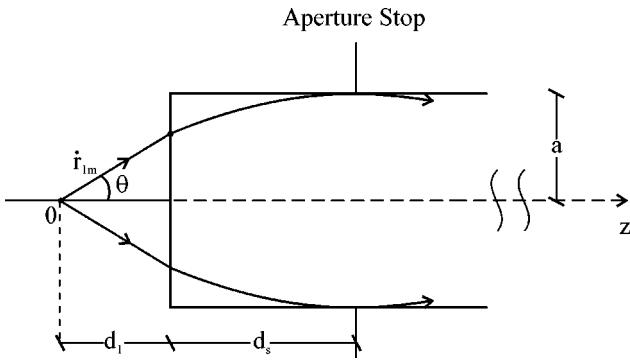


Fig. 4 Aperture stop in a GRIN lens for an on-axis object point.

$$a_e = \frac{n_0 d_1 a}{H_a(d_s) + n_0 d_1 H_f(d_s)}, \quad (31)$$

$$\frac{\dot{H}_f(d_s)}{H_a(d_s)} = -\frac{1}{n_0 d_1}, \quad (32)$$

where Eq. (7) has been used.

Inserting Eq. (32) into Eq. (31) we have

$$a_e = a \dot{H}_a(d_s), \quad (33)$$

where Eq. (4) has been used. Equation (33) indicates that the effective radius is proportional to the slope of the axial ray at d_s , and Eq. (32) provides the aperture stop position given by

$$\tan \left[\int_0^{d_s} g(z') dz' \right] = \frac{1}{n_0 g_0 d_1}, \quad (34)$$

where Eqs. (3) have been used.

Once the position of the aperture stop is known, the entrance and exit pupils can be evaluated.¹¹ The image of the aperture stop formed by the part of the GRIN lens between the aperture stop and the on-axis object will provide the entrance pupil. Thus, by taking into account GRIN lens law and transverse magnifications for an object placed on the input face of a GRIN lens of thickness d_s , the position of the entrance pupil measured from the front face of the GRIN lens can be evaluated⁹

$$d_{\text{enp}} = -\frac{H_a(d_s)}{n_0 \dot{H}_a(d_s)} = \frac{-1}{n_0^2 d_1 g_0 g(d_s)}, \quad (35)$$

and, likewise, the entrance pupil radius can be found

$$a_{\text{enp}} = \frac{a}{\dot{H}_a(d_s)} = \frac{a g_0^{1/2}}{g^{1/2}(d_s) \cos \left[\int_0^{d_s} g(z') dz' \right]}, \quad (36)$$

where Eqs. (3) and (34) have been used. Equation (36), from trigonometric relationship and Eqs. (23) and (34), can be expressed as

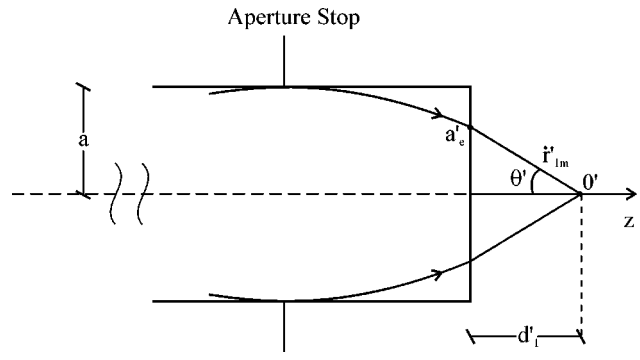


Fig. 5 Limitation of rays in the image space.

$$a_{\text{enp}} = \frac{a(1 + n_0^2 g_0^2 d_1^2)^{1/2}}{g^{1/2}(d_s) n_0 d_1 g_0^{1/2}} = \frac{a^2}{a_e}. \quad (37)$$

On the other hand, the image of the aperture stop formed by the part of the lens between the aperture stop and the image O'_i of the axial object point located at d'_i from the output face of the GRIN lens provides the exit pupil (Fig. 5). Then, the position of this pupil is given by

$$d'_{\text{exp}} = -\frac{H_a(d_s - d)}{n_0 \dot{H}_a(d_s - d)} = \frac{-1}{n_0^2 d'_i g(d) g(d_s)}, \quad (38)$$

and its size by

$$a'_{\text{exp}} = \frac{a}{\dot{H}_a(d_s - d)} = \frac{a^2}{a'_e}, \quad (39)$$

where $a'_e = a_e |F(d)|$ is the output effective radius of the lens. Note also that Eqs. (38) and (39) can be obtained from Eqs. (35) and (37) by replacing g_0 , d_1 , and a_e with $g(d)$, d'_i , and a'_e , respectively.

We now return to off-axis objects. As is shown in Fig. 6, the limitation in the cone of light of an off-axis object point will happen in the plane d''_s for the upper meridional ray and in the plane d'_s for the lower one. The turning position of the upper meridional ray shifts toward the input face of the lens, and for the lower, it moves away from the input face. It acts like an aperture stop that tilts, and there will be

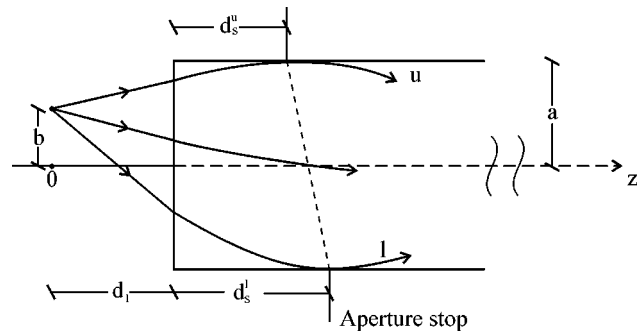


Fig. 6 Aperture stop for an off-axis object point.

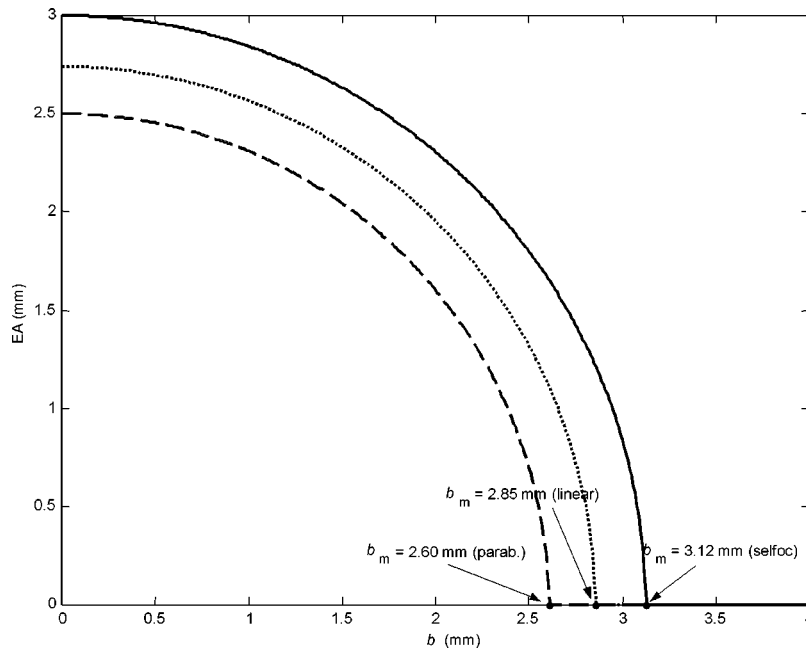


Fig. 7 Effective aperture of a tapered GRIN lens against lateral displacement b of the object point. Three different refractive index profiles have been analyzed: selfoc (solid line), divergent linear (dotted line), and divergent parabolical (dashed line). For each case, the b_m value is shown. Calculations were made for the data cited in Sec. 5.

a gradual loss of light until no image transmission is achieved. This causes vignetting, which completely blocks rays for off-axis points higher than a threshold height of the object.

Extreme positions of the aperture stop for the upper and lower marginal rays can be evaluated from the conditions of Eq. (30) to give

$$a_e^{(u)} = \pm a \dot{H}_a \left[d_s^{(u)} \right]. \tag{40}$$

Substituting Eq. (3b) into Eq. (40), the extreme positions of the aperture stop are given by

$$\int_0^{d_s^{(u)}} g(z') dz' = \cos^{-1} \left\{ \frac{g_0^{1/2} a_e^{(u)}}{a g^{1/2} \left[d_s^{(u)} \right]} \right\}. \tag{41}$$

Moreover, the position of the center of the tilted aperture stop is the position d_s^c on the optical axis at which the chief ray crosses it. For the center position, $r_{ch}(d_s^c) = 0$ and Eq. (17) reduces to

$$\tan \left[\int_0^{d_s^c} g(z') dz' \right] = \frac{1}{n_0 g_0 d_1}, \tag{42}$$

where Eqs. (3) have been used. The position d_s^c resulting from Eq. (42) coincides with the position of the aperture stop for an on-axis object point.

5 Results

There are different kinds of tapered GRIN lenses depending on the functional form of $g(z)$. In this section, the study

developed so far is applied to two refractive index profiles and compared with the well-known selfoc lenses.

Let us begin regarding lenses with divergent linear and parabolical taper functions (whose importance as focusers and in optical communications must be emphasized) given, respectively, by

$$g(z) = \frac{g_0}{1 + z/L} \quad \text{and} \quad g(z) = \frac{g_0}{(1 + z/L)^2}, \tag{43}$$

where L is the distance from $z=0$ to the common apex of the equi-index lines, and $g_0 = g(0)$.

We first analyze how the effective and numerical apertures evolve according to their dependence on different variables. Calculations are made for lens radius $a = 2.5$ mm, GRIN lens thickness $d = 7$ mm, index at the optical axis $n_0 = 1.5$, $g_0 = 0.1 \text{ mm}^{-1}$, and $L = 100$ mm; then again, object lateral displacement $b = 1$ mm, distance $d_1 = 5$ mm, and $z = 20$ mm except for those cases in which we are interested in studying a magnitude as a function of either of the three of them.

In Fig. 7, the evolution of the effective aperture in terms of the object lateral displacement b is presented. The EA decreases as the object point moves off the axis and up to a height equal to b_m (maximum spatial extension of the object which contributes to the image formation), calculated from Eq. (20), where it vanishes. Here b_m has values 2.85 and 2.60 mm, respectively, for the linear and parabolical lens with the aforementioned parameters.

Figure 8(a) shows the evolution of the EA as the object moves backwards away from the input face of the GRIN

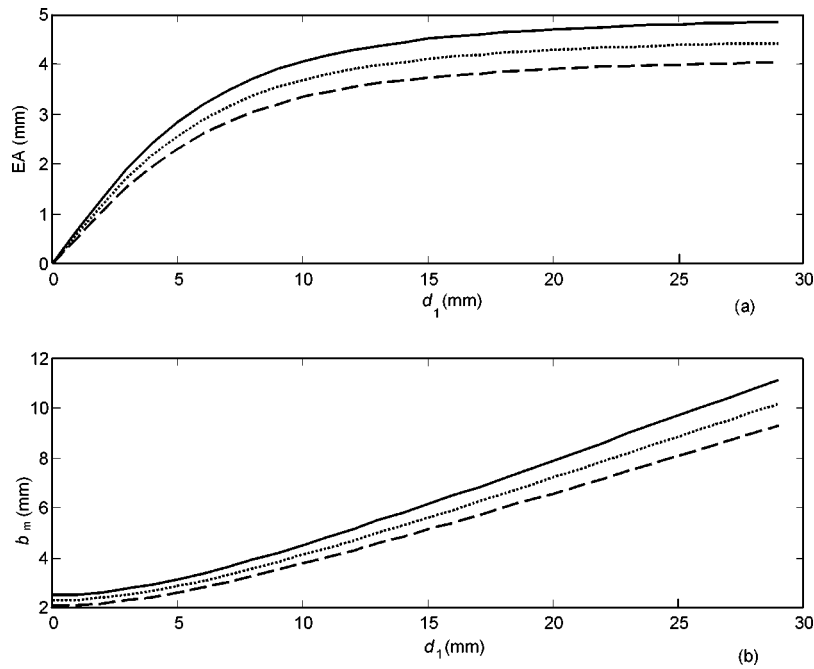


Fig. 8 Variation of the EA with object distance d_1 from the input face of the lens. A plot of the EA against d_1 is shown (a) as well as how high b_m becomes as d_1 increases (b). Again, the solid line is for a selfoc lens, the dotted line is for a divergent linear lens, and the dashed line is for the divergent parabolical one.

lens. It varies from zero for $d_1=0$ up to a value that can be obtained for $d_1 \rightarrow \infty$ by solving

$$EA_{(d_1 \rightarrow \infty)} = 2a \left[\frac{g(z)}{g_0} \right]^{1/2}, \tag{44}$$

which is 4.56 mm for the linear lens and 4.17 mm for the parabolical one.

In Fig. 8(b) we observe that b_m increases with d_1 , being $ag(z)/g_0$ its value for $d_1=0$. This means that the more separated the object is from the input face of the lens, the higher will be the maximum spatial extension. This is important for the achievement of the most detailed image, trying to diminish vignetting as much as possible.

Now consider Eq. (19). EA assumes a real value for certain values of taper function $g(z)$ and thickness z . This defines an interval that goes from $z=0$ to $z=z_{\max}$ or, equivalently, from $g(z)=g_0$ to $g(z)=g(z)_{\min}$, where $g(z)_{\min}$ is

$$g(z)_{\min} = \frac{g_0^2 b^2}{a^2 g_0 (1 + n_0^2 g_0^2 d_1^2)}. \tag{45}$$

For the particular case studied $g(z)_{\min} = 0.0102 \text{ mm}^{-1}$, which implies that z_{\max} equals 880.34 and 213.11 mm, respectively, depending on the index profile. In Figs. 9(a) and 9(b) this dependence is shown and we can deduce from these figures that the dependence shows reverse behaviors: when the EA is plotted against $g(z)$, it goes from zero up to a maximum value obtained for g_0 , whereas it decreases until it cancels at z_{\max} when z is the independent variable.

For an on-axis object, it is possible to calculate the input numerical aperture (NA_{in}) and see how it changes with the variables on which it depends. In Fig. 10 we can see that NA_{in} decreases as d_1 increases, going to zero as d_1 stretches to infinity. On the other hand, Fig. 11 shows how NA_{in} evolves with gradient parameter $g(z)$ and z . For the sake of comparison, we can take into account Fig. 9. The main difference between them is that in this case there is no upper limitation for z , which implies there is no minimum value for the taper function. As a consequence, NA_{in} varies from zero to a maximum value for $g(z)=0$ and $g(z)=g_0$, respectively, and it presents reverse behavior for $z=0$ and $z \rightarrow \infty$.

In all cases, the EA and NA_{in} are higher for the linear profile than for the parabolical profile, and even higher for the selfoc lens, but they present parallel behaviors for all cases.

Next, we study characteristics regarding aperture stop and input and output pupils. From Eq. (34), the expressions of the position of the aperture stop for the two profiles can be deduced. These are

$$d_s^l = L \left\{ \exp \left[\frac{1}{g_0 L} \tan^{-1} \left(\frac{1}{n_0 g_0 d_1} \right) \right] - 1 \right\}, \tag{46}$$

for the divergent linear lens, and

$$d_s^p = L \left\{ \left[1 - \frac{1}{g_0 L} \tan^{-1} \left(\frac{1}{n_0 g_0 d_1} \right) \right]^{-1} - 1 \right\}, \tag{47}$$

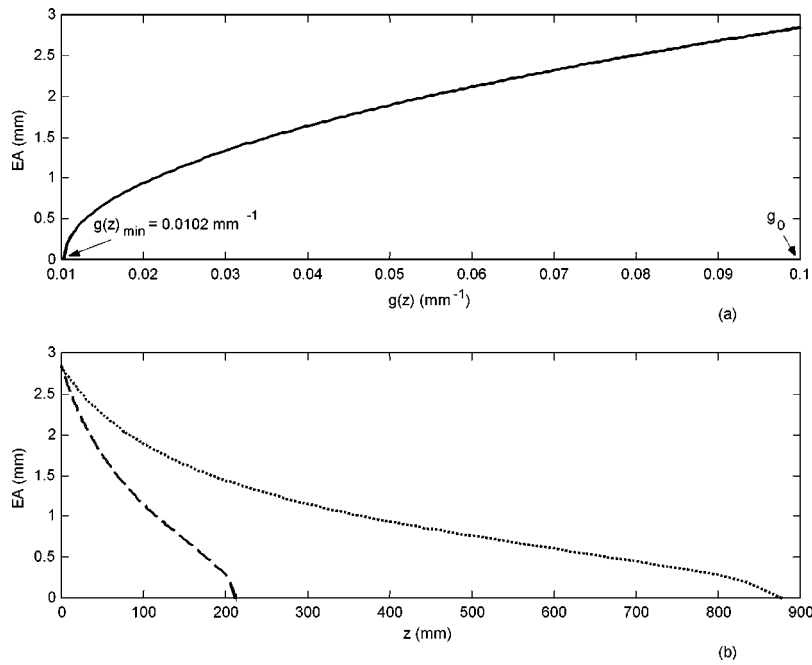


Fig. 9 EA of a tapered GRIN lens against (a) gradient parameter $g(z)$ and (b) thickness z . In (b), the dotted line is for a divergent linear lens and the dashed line is for a divergent parabolical lens.

for the divergent parabolical lens. Both of these tend to zero as d_1 tends to infinity, whereas when $d_1=0$, they reach values given by

$$d_{s(d_1=0)}^l = L \left[\exp\left(\frac{\pi}{2g_0L}\right) - 1 \right], \tag{48}$$

and

$$d_{s(d_1=0)}^p = L \pi / (2g_0L - \pi). \tag{49}$$

Figure 12 shows the dependence of d_s on d_1 . We can observe that d_s decreases with d_1 .

In Figs. 13 and 14, the evolution of the entrance and exit pupil radii, whose expressions are given by Eqs. (36) and (39), respectively, are seen with d_s and d_1 . The entrance

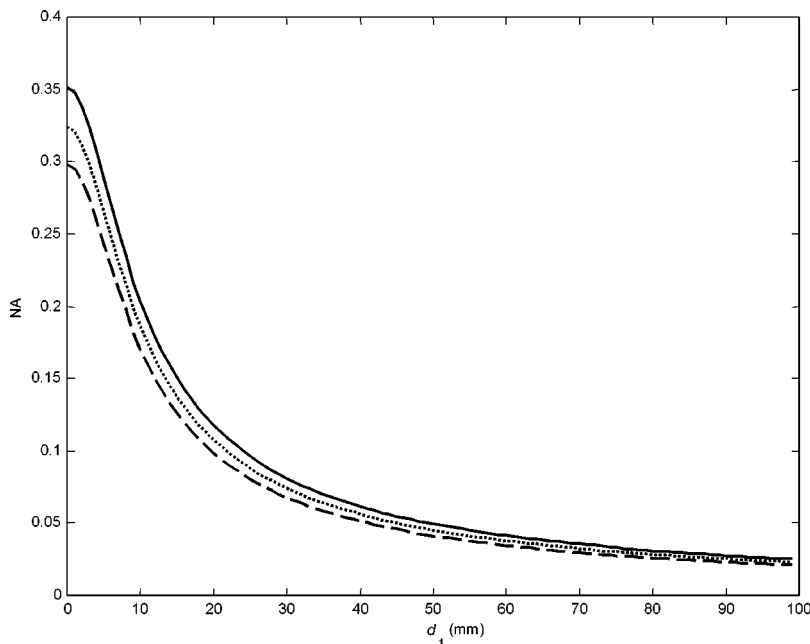


Fig. 10 Relationship between the input numerical aperture (NA_{in}) and object distance d_1 for a selfoc lens (solid line), a divergent linear lens (dotted line), and a divergent parabolical lens (dashed line).

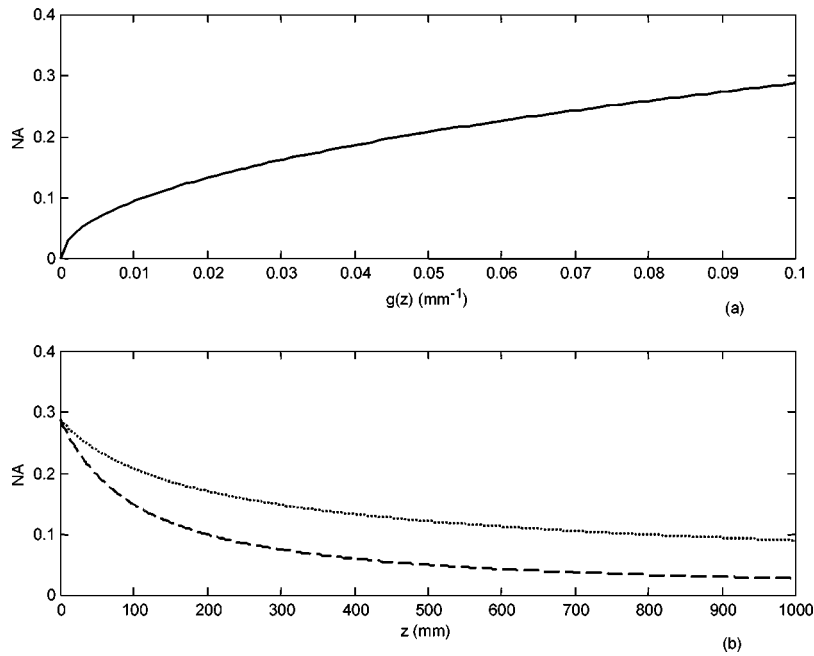


Fig. 11 NA_{in} of a tapered GRIN lens against (a) gradient parameter $g(z)$ and (b) thickness z . In (b), the dotted line is for a divergent linear lens and the dashed line is for a divergent parabolical lens.

pupil radius a_{enp} increases with increasing d_s , departing from a value equal to the physical radius of the lens, obtained for $d_s=0$ ($d_1 \rightarrow \infty$), and going to a value $d_s^{max}(d_1=0)$ such that

$$\int_0^{d_s} g(z') dz' = \pi/2. \tag{50}$$

The relationship between a_{enp} and d_1 is a reciprocal one.

The exit pupil radius a'_{exp} presents radically different behavior. It spreads over the same range of values as in Fig. 13, starting at $d_s=0$ ($d_1 \rightarrow \infty$) where a'_{exp} is

$$a'_{exp(d_1 \rightarrow \infty)} = a \left[\frac{g(d)}{g_0} \right]^{1/2} \left\{ \cos \left[\int_0^d g(z') dz' \right] \right\}^{-1}, \tag{51}$$

and ending up at $d_1=0$, or d_s such that Eq. (50) verifies, with a value

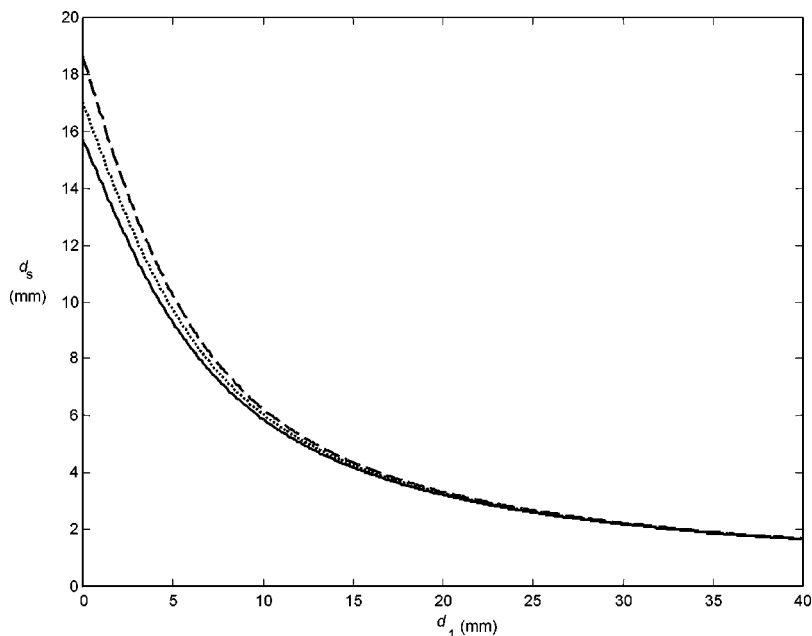


Fig. 12 Dependence of aperture stop position d_s on object distance d_1 for the three refractive index profiles in Fig. 7.

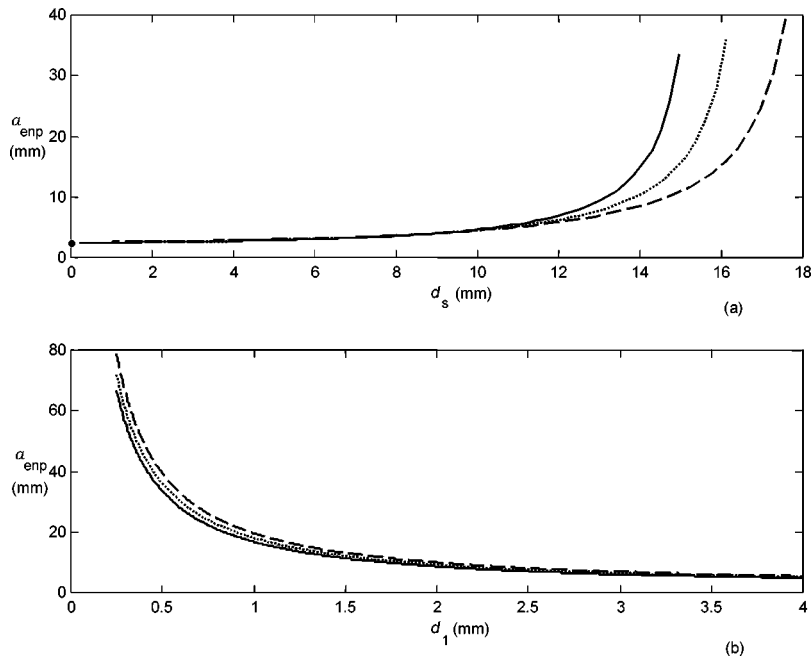


Fig. 13 Entrance pupil radius a_{enp} against (a) aperture stop position d_s and (b) object distance d_1 for the three refractive index profiles in Fig. 7.

$$a'_{\text{exp}(d_1=0)} = a \left[\frac{g(d)}{g(d_s)} \right]^{1/2} \left\{ \sin \left[\int_0^d g(z') dz' \right] \right\}^{-1}. \quad (52)$$

All the curves intersect for $d_s = d$, the value for which a selfoc lens reaches its minimum exit pupil radius ($a'_{\text{exp}} = a$).

Now that the positions of the aperture stop for on-axis

objects have been studied, it is time to extend the study to include off-axis objects and see how the aperture stop tilts. As already noted, the center of the tilting aperture stop coincides with the position d_s for on-axis objects, which was analyzed in Fig. 12. From Eq. (41), the upper and lower positions of the tilted aperture stop can be extracted. Their representation can be observed in Fig. 15: the upper position shifts toward the front of the lens while the lower

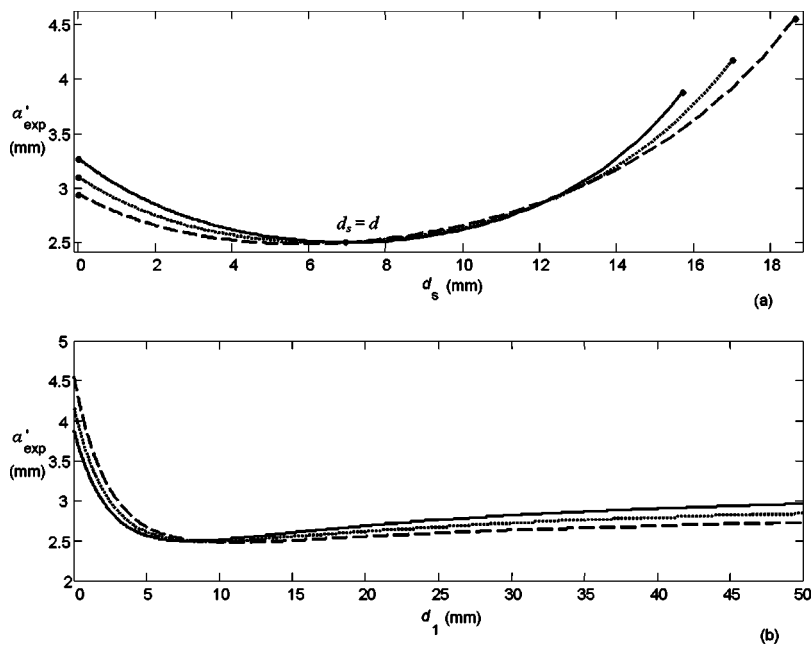


Fig. 14 Exit pupil radius a'_{exp} against (a) aperture stop position d_s and (b) object distance d_1 for the three refractive index profiles in Fig. 7.

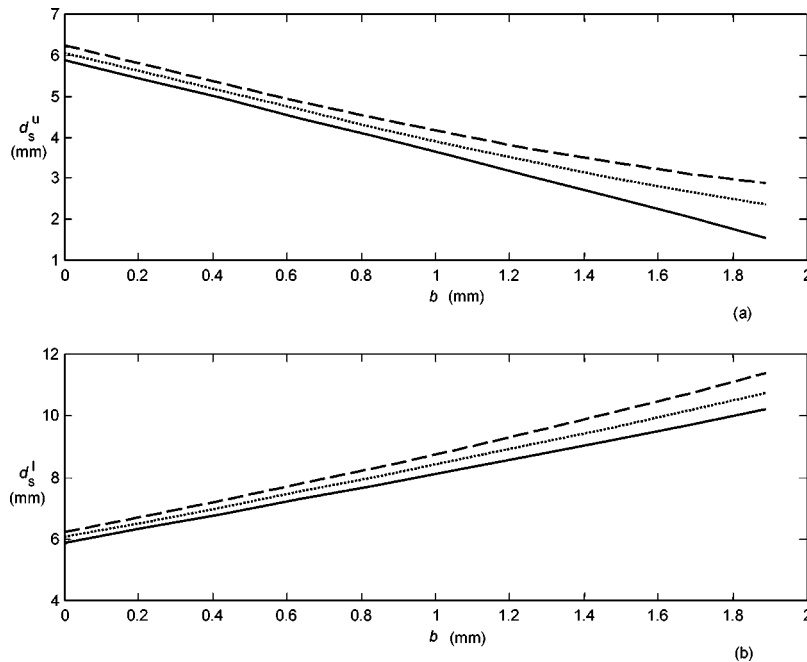


Fig. 15 (a) Upper and (b) lower positions of the tilted aperture stop (d_s^u and d_s^l) against the lateral displacement b of the object point for a selfoc lens (solid line), a divergent linear lens (dotted line), and a divergent parabolic lens (dashed line).

one shifts toward the back, both forming a straight line that goes through center position d_s .

6 Conclusions

Equations for the marginal rays, effective aperture and NA, aperture stop, pupils, and size of the field of view in tapered GRIN lenses were derived. The results obtained were applied to GRIN lenses with divergent linear and parabolic taper functions as well as compared to selfoc lenses. The knowledge of these topics should be useful for designing tapered GRIN systems.

Acknowledgments

This work was supported by the Xunta de Galicia, Spain, under Contract PGIDT99PXI22201B.

References

1. F. P. Kapron, "Geometrical optics of parabolic gradient-index cylindrical lenses," *J. Opt. Soc. Am.* **60**(11), 1433–1436 (1970).
2. E. W. Marchand, "Ray tracing in gradient index media," *J. Opt. Soc. Am.* **60**(1), 1–7 (1970).
3. W. Streifer and K. P. Paxton, "Analytic solution of ray equations in cylindrically inhomogeneous guiding media. 1: Meridional rays," *Appl. Opt.* **10**(4), 769–775 (1971).
4. S. J. S. Brown, "Geometrical optics of tapered gradient-index rods," *Appl. Opt.* **19**(7), 1056–1060 (1980).
5. J. R. Flores, C. Gómez-Reino, E. Acosta, and J. Liñares, "Geometrical optics of gradient index lenses," *Opt. Eng.* **28**(11), 1173–1179 (1989).
6. C. Gómez-Reino and E. Larrea, "Pupil effect in GRIN material," *Appl. Opt.* **22**(7), 970–973 (1983).
7. M. E. Harrigan, "Some first-order properties of radial gradient lenses compared to homogeneous lenses," *Appl. Opt.* **23**(16), 2702–2705 (1984).
8. E. Acosta, C. Gómez-Reino, and J. Liñares, "Effective radius and numerical aperture of GRIN lenses with revolution symmetry," *Appl. Opt.* **26**(15), 2952–2955 (1987).
9. C. Gómez-Reino, E. Acosta, and M. V. Pérez, "Limitation in the cone of light through GRIN lenses: stops, pupils and vignetting," *Jpn. J. Appl. Phys., Part 1* **31**(5B), 1582–1585 (1992).
10. K. Iga, Y. Kokubun, and M. Oikawa, "Image transmission and transformation," Chap. 5 in *Fundamentals of Microoptics*, Academic Press, New York (1984).
11. M. H. Freeman, *Optics*, Chap. 5, Butterworths, London (1990).



José Manuel Rivas-Moscoco received his BS and MS degrees in physics in 1998 and 1999, respectively, from the University of Santiago de Compostela, where he is currently working toward his PhD degree in graded-index optics.



Carlos Gómez-Reino received his BS, MS, and PhD degrees in physics in 1968, 1970, and 1975, respectively, from the Complutense University of Madrid, where from 1970 to 1979 he was an assistant professor. He has been a professor of optics with the Faculty of Physics and Optics and Optometry School, University of Santiago de Compostela, since 1980. He has published more than 120 papers in the areas of zone plates, integrated optics, and graded-index optics. He is a member of the Spanish Royal Society of Physics, the Spanish Society of Optics, OSA, SPIE, AAAS, and the New York Academy of Sciences and a fellow of OSA.

María Victoria Pérez Martín received her BS and MS degrees in physics in 1969 and 1970, respectively, from the Complutense University of Madrid, where from 1971 to 1979 she was an assistant

professor. She received her PhD degree in physics in 1985 from the University of Santiago de Compostela (USC). She has been a professor of optics at the USC since 1987. She has published more than 60 papers in the areas of zone plates, graded-index optics, and optometry.

Carmen Bao Varela received her BS, MS, and PhD degrees in physics in 1993, 1994, and 1997, respectively, from the University of Santiago de Compostela (USC). She has been an assistant professor at the USC since 1998. She has published 30 papers in the areas of integrated optics and graded-index optics.